

A SPECTRAL SCHEME FOR VISCOELASTIC SEISMIC MODELING

James C. Schatzman and Zhaobo Meng

Department of Mathematics, University of Wyoming, P.O. Box 3036, Laramie, WY 82071
(307) 766-3208; jcs@uwyo.edu

Sponsored by AFOSR F49620-94-1-0134 and F49620-94-1-0408

ABSTRACT

The pseudospectral method is especially valuable for seismic modeling because of its high accuracy compared to other numerical techniques. The method can be regarded as a limit of finite difference of increasing orders, and a process of trigonometric interpolation, thus it exhibits high accuracy. Stability of the method is also favorable. Fourier polynomials are especially efficient but have the disadvantage of forcing periodicity, and Chebyshev polynomials are somewhat less efficient but are more flexible in application of boundary conditions. We have used a Fourier pseudospectral method in the horizontal direction and Chebychev polynomials in the vertical direction. Curved grids conforming to the surface topography and major interfaces are made possible by coordinate transformations. A full viscoelastic formulation permits convenient implementation of attenuating layers to reduce wrap-around in the horizontal direction. The result is an efficient method for 2- and 3-D linear viscoelastic wave propagation.

Key Words viscoelastic, wave propagation, seismic modeling

1. Objective

1.1. Introduction

Anelasticity and anisotropy of the earth play important roles in wave propagation, especially when waves travel long distances. Finite difference and finite element methods suffer from inaccuracies in the form of numerical dispersion and attenuation that make it difficult to simulate wave propagation over hundreds to thousands of wavelengths. The pseudospectral method exhibits very striking features of very low grid density and high efficiency, compared to the standard Cartesian discrete methods. The goal here is to simulate wave propagation in a region of about 2,000 km in azimuth and 100-200 km in depth; source frequencies are 0.5-10 Hz. Since wavelengths range from 120-4,000 meters, this represents propagation of about 500-20,000 wavelengths. Most FD or FE schemes either exhibit excessive numerical artifacts or are very inefficient for such problems.

Due to space limitations, we describe only the isotropic 2-D formulation. However, the anisotropic 3-D case is a straightforward extension and a detailed analysis is available from the authors.

1.2. 2-D Viscoelastic Wave Equations

When we talk about viscoelasticity, there are mainly two different ways to describe the strain–stress relationship, i.e. Voigt's model or Maxwell's model, each corresponding to connections of the elastic and viscous behavior in parallel and series. For computational consideration, Voigt's model is highly recommended because of its simplicity and generality.

For an isotropic-elastic medium the stress-strain relation is

$$\sigma_{ii} = \bar{\lambda}\Delta + 2\bar{\mu}\varepsilon_{ii}, \quad i = 1, 2, 3, \quad (1)$$

$$\sigma_{ij} = \bar{\mu}\varepsilon_{ij}, \quad i \neq j, \quad i, j = 1, 2, 3, \quad (2)$$

where $\bar{\lambda} = \lambda + \lambda' \frac{\partial}{\partial t}$ and $\bar{\mu} = \mu + \mu' \frac{\partial}{\partial t}$. It is beyond the scope of this paper to include a derivation, but we find that λ' and μ' are related to the Q for P- and S-wave propagation by

$$Q_p = \frac{\sqrt{(\lambda + 2\mu)^2 + k^2(\lambda' + 2\mu')^2 v_p^2} + \lambda + 2\mu}{2(\lambda' + 2\mu')k v_p}. \quad (3)$$

$$Q_s = \frac{\sqrt{\mu^2 + k^2\mu'^2 v_s^2} + \mu}{2\mu'k v_s}. \quad (4)$$

We see that in this model, Q_p and Q_s are not constant but are functions of wavenumber. The viscoelastic equations of motion are

$$\rho \frac{\partial^2 u_i}{\partial t^2} = \frac{\partial}{\partial x_i} [(\bar{\lambda} + \bar{\mu})\theta] + \nabla \cdot (\bar{\mu}\nabla u_i) + f_i, \quad i = 1, 2, 3, \quad (5)$$

where $\mathbf{f} = (f_1, f_2, f_3)^T$ is the applied force.

If in a region the medium is partially homogeneous (μ and μ' are constants), then in this region we have

$$\rho \frac{\partial^2 \theta}{\partial t^2} = (\bar{\lambda} + 2\bar{\mu})\Delta\theta, \quad (6)$$

and

$$\rho \frac{\partial^2 \omega}{\partial t^2} = \bar{\mu}\Delta\omega. \quad (7)$$

where $\theta = \nabla \cdot \mathbf{u}$ and $\omega = \nabla \times \mathbf{u}$. Thus we see that even in viscoelastic media the dilation wave equation is similar to a “pure” P-wave equation and the rotational wave equations coincides in form with the “pure” S-wave equation.

1.3. 2-D Isotropic Viscoelastic Wave Equations

For a 2-D isotropic viscoelastic medium, we have

$$\rho \frac{\partial^2 u_1}{\partial t^2} = \frac{\partial}{\partial x_1} \left[(\bar{\lambda} + \bar{\mu}) \left(\frac{\partial u_1}{\partial x_1} + \frac{\partial u_3}{\partial x_3} \right) \right] + \frac{\partial}{\partial x_1} \left(\bar{\mu} \frac{\partial u_1}{\partial x_1} \right) + \frac{\partial}{\partial x_3} \left(\bar{\mu} \frac{\partial u_1}{\partial x_3} \right) + f_1, \quad (8)$$

and

$$\rho \frac{\partial^2 u_3}{\partial t^2} = \frac{\partial}{\partial x_3} \left[(\bar{\lambda} + \bar{\mu}) \left(\frac{\partial u_1}{\partial x_1} + \frac{\partial u_3}{\partial x_3} \right) \right] + \frac{\partial}{\partial x_1} \left(\bar{\mu} \frac{\partial u_3}{\partial x_1} \right) + \frac{\partial}{\partial x_3} \left(\bar{\mu} \frac{\partial u_3}{\partial x_3} \right) + f_3. \quad (9)$$

We then rewrite these equations as a system of four first order equations:

$$\frac{\partial u_1}{\partial t} = v_1, \quad (10)$$

$$\frac{\partial u_3}{\partial t} = v_3, \quad (11)$$

$$\begin{aligned} \rho \frac{\partial v_1}{\partial t} &= \frac{\partial}{\partial x_1} \left[(\lambda + \mu) \left(\frac{\partial u_1}{\partial x_1} + \frac{\partial u_3}{\partial x_3} \right) \right] + \frac{\partial}{\partial x_1} \left(\mu \frac{\partial u_1}{\partial x_1} \right) + \frac{\partial}{\partial x_3} \left(\mu \frac{\partial u_1}{\partial x_3} \right) \\ &+ \frac{\partial}{\partial x_1} \left[(\lambda' + \mu') \left(\frac{\partial v_1}{\partial x_1} + \frac{\partial v_3}{\partial x_3} \right) \right] + \frac{\partial}{\partial x_1} \left(\mu' \frac{\partial v_1}{\partial x_1} \right) + \frac{\partial}{\partial x_3} \left(\mu' \frac{\partial v_1}{\partial x_3} \right) + f_1, \end{aligned} \quad (12)$$

$$\begin{aligned} \rho \frac{\partial v_3}{\partial t} &= \frac{\partial}{\partial x_3} \left[(\lambda + \mu) \left(\frac{\partial u_1}{\partial x_1} + \frac{\partial u_3}{\partial x_3} \right) \right] + \frac{\partial}{\partial x_1} \left(\mu \frac{\partial u_3}{\partial x_1} \right) + \frac{\partial}{\partial x_3} \left(\mu \frac{\partial u_3}{\partial x_3} \right) \\ &+ \frac{\partial}{\partial x_3} \left[(\lambda' + \mu') \left(\frac{\partial v_1}{\partial x_1} + \frac{\partial v_3}{\partial x_3} \right) \right] + \frac{\partial}{\partial x_1} \left(\mu' \frac{\partial v_3}{\partial x_1} \right) + \frac{\partial}{\partial x_3} \left(\mu' \frac{\partial v_3}{\partial x_3} \right) + f_3, \end{aligned} \quad (13)$$

The 2-D forward modeling problem consists of solving equations (24–27) in rectangular domains with a free surface on $x_3 = X_S(x_1)$. The equations for zero normal and tangential surface stress are respectively:

$$(\lambda + 2\mu) \frac{\partial u_3}{\partial x_3} + \lambda \frac{\partial u_1}{\partial x_1} + (\lambda' + 2\mu') \frac{\partial v_3}{\partial x_3} + \lambda' \frac{\partial v_1}{\partial x_1} = 0, \quad (14)$$

$$\mu \left(\frac{\partial u_1}{\partial x_3} + \frac{\partial u_3}{\partial x_1} \right) + \mu' \left(\frac{\partial v_1}{\partial x_3} + \frac{\partial v_3}{\partial x_1} \right) = 0. \quad (15)$$

We choose radiation boundary conditions at the bottom:

$$\prod_{a=p,s} \prod_{j=1}^J \left[\alpha_a(x_1, x_3) + \cos \phi_j^a(x_1, x_3) \frac{\partial}{\partial x_1} + \sin \phi_j^a(x_1, x_3) \frac{\partial}{\partial x_3} + n \frac{1}{v_a(x_1, x_3)} \frac{\partial}{\partial t} \right] \begin{pmatrix} u_1 \\ u_3 \end{pmatrix} = 0, \quad (16)$$

where $|\phi_j| < \pi/2$, $j = 1, 2, \dots, J$. The radiation boundary conditions (30) are imposed such that the wave motions from the interior of the domain to pass through the boundary $x_3 = X_B(x_1)$ without being reflected. In general it is not possible to find practical boundary conditions that do the above task perfectly, however, the artificial reflections can be substantially reduced. Any linear combination of plane waves traveling out of the boundary $x_3 = X_B(x_1)$ at angles of incidence $\pm\phi_1, \pm\phi_2, \dots, \pm\phi_J$ with speed v_a satisfies these boundary conditions (Higdon, 1987), where the absorption coefficients (Meng et al., 1989) are

$$\alpha_p = \frac{(\lambda + 2\mu)'_s}{2(\lambda + 2\mu)} + \frac{\omega^2 \sqrt{\rho} (\lambda' + 2\mu')}{2(\lambda + 2\mu)^{3/2}}, \quad (17)$$

$$\alpha_s = \frac{\mu'_s}{2\mu} + \frac{\omega^2 \mu' \sqrt{\rho}}{2\mu^{3/2}}, \quad (18)$$

No explicit boundary conditions are use on the sides. The natural (periodic) conditions are employed for Fourier polynomials. Absorption is accomplished by using hin absorbing layers with μ' and λ' gradually increasing towards the boundaries.

To obtain a rectangular geometry for a problem with an irregular top and bottom (due to surface topography and curvature of the earth) we employ a transformation from (x_1, x_3) to (x_1, η) , where $\eta = \eta(x_1, x_3)$ (Fig. 1). The equations of motion then become

$$\frac{\partial u_1}{\partial t} = v_1, \quad (19)$$

$$\frac{\partial u_3}{\partial t} = v_3, \quad (20)$$

$$\begin{aligned} \rho \frac{\partial v_1}{\partial t} &= \left(\frac{\partial}{\partial x_1} + \eta_{x_1} \frac{\partial}{\partial \eta} \right) \left[(\lambda + \mu) \left(\frac{\partial u_1}{\partial x_1} + \eta_{x_1} \frac{\partial u_1}{\partial \eta} + \eta_{x_3} \frac{\partial u_3}{\partial \eta} \right) \right] \\ &+ \left(\frac{\partial}{\partial x_1} + \eta_{x_1} \frac{\partial}{\partial \eta} \right) \left[\mu \left(\frac{\partial u_1}{\partial x_1} + \eta_{x_1} \frac{\partial u_1}{\partial \eta} \right) \right] + \left(\eta_{x_3} \frac{\partial}{\partial \eta} \right) \left[\mu \left(\eta_{x_3} \frac{\partial u_1}{\partial \eta} \right) \right] \\ &+ \left(\frac{\partial}{\partial x_1} + \eta_{x_1} \frac{\partial}{\partial \eta} \right) \left[(\lambda' + \mu') \left(\frac{\partial v_1}{\partial x_1} + \eta_{x_1} \frac{\partial v_1}{\partial \eta} + \eta_{x_3} \frac{\partial v_3}{\partial \eta} \right) \right] \\ &+ \left(\frac{\partial}{\partial x_1} + \eta_{x_1} \frac{\partial}{\partial \eta} \right) \left[\mu' \left(\frac{\partial v_1}{\partial x_1} + \eta_{x_1} \frac{\partial v_1}{\partial \eta} \right) \right] + \left(\eta_{x_3} \frac{\partial}{\partial \eta} \right) \left[\mu' \left(\eta_{x_3} \frac{\partial v_1}{\partial \eta} \right) \right] + f_1 \end{aligned} \quad (21)$$

$$\begin{aligned} \rho \frac{\partial v_3}{\partial t} &= \left(\eta_{x_3} \frac{\partial}{\partial \eta} \right) \left[(\lambda + \mu) \left(\frac{\partial u_1}{\partial x_1} + \eta_{x_1} \frac{\partial u_1}{\partial \eta} + \eta_{x_3} \frac{\partial u_3}{\partial \eta} \right) \right] \\ &+ \left(\frac{\partial}{\partial x_1} + \eta_{x_1} \frac{\partial}{\partial \eta} \right) \left[\mu \left(\frac{\partial u_3}{\partial x_1} + \eta_{x_1} \frac{\partial u_3}{\partial \eta} \right) \right] + \left(\eta_{x_3} \frac{\partial}{\partial \eta} \right) \left[\mu \left(\eta_{x_3} \frac{\partial u_3}{\partial \eta} \right) \right] \\ &+ \left(\eta_{x_3} \frac{\partial}{\partial \eta} \right) \left[(\lambda' + \mu') \left(\frac{\partial v_1}{\partial x_1} + \eta_{x_1} \frac{\partial v_1}{\partial \eta} + \eta_{x_3} \frac{\partial v_3}{\partial \eta} \right) \right] \\ &+ \left(\frac{\partial}{\partial x_1} + \eta_{x_1} \frac{\partial}{\partial \eta} \right) \left[\mu' \left(\frac{\partial v_3}{\partial x_1} + \eta_{x_1} \frac{\partial v_3}{\partial \eta} \right) \right] + \left(\eta_{x_3} \frac{\partial}{\partial \eta} \right) \left[\mu' \left(\eta_{x_3} \frac{\partial v_3}{\partial \eta} \right) \right] + f_3 \end{aligned} \quad (22)$$

The free surface boundary conditions at the top become:

$$(\lambda + 2\mu) \left(\eta_{x_3} \frac{\partial u_3}{\partial \eta} \right) + \lambda \left(\frac{\partial u_1}{\partial x_1} + \eta_{x_1} \frac{\partial u_1}{\partial \eta} \right) + (\lambda' + 2\mu') \left(\eta_{x_3} \frac{\partial v_3}{\partial \eta} \right) + \lambda' \left(\frac{\partial v_1}{\partial x_1} + \eta_{x_1} \frac{\partial v_1}{\partial \eta} \right) = 0 \quad (23)$$

$$\mu \left(\eta_{x_3} \frac{\partial u_1}{\partial \eta} + \frac{\partial u_3}{\partial x_1} + \eta_{x_1} \frac{\partial u_3}{\partial \eta} \right) + \mu' \left(\eta_{x_3} \frac{\partial v_1}{\partial \eta} + \frac{\partial v_3}{\partial x_1} + \eta_{x_1} \frac{\partial v_3}{\partial \eta} \right) = 0 \quad (24)$$

The radiation boundary conditions at the bottom take the form

$$\alpha_1 + \cos \phi \left(\frac{\partial u_1}{\partial x_1} + \eta_{x_1} \frac{\partial u_1}{\partial \eta} \right) + \sin \phi \left(\eta_{x_3} \frac{\partial u_1}{\partial \eta} \right) + \frac{v_1}{v} = 0, \quad (25)$$

$$\alpha(x_1, x_3) u_3 + \cos \phi(x_1, x_3) \left(\frac{\partial u_3}{\partial x_1} + \eta_{x_1} \frac{\partial u_3}{\partial \eta} \right) + \sin \phi(x_1, x_3) \left(\eta_{x_3} \frac{\partial u_3}{\partial \eta} \right) + \frac{v_3}{v(x_1, x_3)} = 0. \quad (26)$$

These equations are to be approximated through collocation and quadrature (we use fourth order Runge-Kutta). The solutions are represented as 2-D discrete Fourier-Chebyshev transforms in (x_1, η) . Differentiations with respect to x_1 and η are carried out in the usual way. The η derivatives of u_1 , u_3 , v_1 and v_3 result in four unknowns per k_x value: the $4N_x$ highest Chebyshev modes are lost in the differentiation process. In principal, these are to be determined by the $4N_x$ top and bottom boundary conditions. Due to the higher derivatives in the equations of motion, there are actually a total of $14N_x$ unknown highest Chebyshev modes. The highest modes in the equations are irrelevant and are ignored. Instead, the highest modes in the $4N_x$ unknowns are updated according to the $4N_x$ top and bottom boundary conditions.

Stability of Runge-Kutta for this problem has been studied. Details are available from the authors.

1.4. About the Grids

The strategy adopted for choosing the mapping function η is to flatten the surface and major contours. "Major contours" are those interfaces, typically the basement and moho, that are continuous across the section. Fig. 1 shows one of a set of "deep sedimentary basin" models that are being tested. Fig. 2 shows a model, derived from seismic data, for a trans-Urals DSS path.

Once the "major contours" are identified, the average travel time between the contours is computed (p-waves have been used so far), and constant values of η are assigned to the major contours so that the differences in η are proportional to the travel time. In this way, increments of constant $\Delta\eta$ correspond roughly to equal increments of travel time. This is done so as to improve the stability properties of the time integration.

1.5. Preliminary Results

Preliminary calculations indicate that it is practical to simulate wave propagation for 2-D models of about 2,000 by 200 km. Such simulations require several days of computation on a SGI Power Challenge (300 MFlops).

We are in the process of quantifying the effects of particular types of crustal features on regional waveforms. Features under study include deep sedimentary basins (see Fig. 1), moho uplift and lateral variation in surface features. Also, some realistic models (such as the Soviet DSS model in Fig. 2) are currently being tested.

2. Recommendations and Future Plans

Other authors have performed simulations for particular models (e.g., Jih (1994) uses a finite difference method); there is not yet completed a comprehensive and quantitative study of the effects of crustal features. Our plan is to use a series of models, for example the deep sedimentary basin models, varying the size and elastic parameters of the basin, to determine how the effects of such basins on crustal wave propagation, such as attenuation of L_g , depend on the parameters of the basin. Additionally, we will study the effects of moho uplift, combined basin and uplift, and surface topographical roughness and other surface features.

One weakness of this method is that, because of its 2-D nature, amplitudes and decay times are not correct, and relative amplitudes of differing phases are not readily obtainable. Although the method described in this paper can readily be applied to the 3-D problem, it is apparent that elastic wavefield computations in a region of 2,000 by 2,000 by 200 km are not practical with any computer available to the authors. However, two acceleration techniques may be employed when solving the problem of wave propagation between two points (source and receiver):

1. Model only a narrow channel between the source and receiver (see Fig. 3). Use absorbing boundary conditions on the lateral boundaries to avoid reflections or wrap-around.
2. Use smaller tracking grids that follows the major wave fronts. A full simulation would then require several runs, each to capture the modes with essentially different paths, but each run would be much quicker than a global computation.

1. Bayliss, A., Jordan, K. E., Lemesurier, B. J. and Turkel, E., 1986, A fourth-order accurate finite-difference scheme for the computation of elastic waves: *Bulletin of the Seismological Society of America*, 76, pp. 1115–1132.
2. Carcione, J. M., 1992, Modeling anelastic singular surface waves in the earth: *Geophysics*, 57, pp. 781–792.
3. Carcione, J. M., Kosloff, D. and Kosloff, R., 1988, Wave propagation simulation in an elastic anisotropic (transversely isotropic) solid: *Q. J. Mech. Appl. Math.*, 41, pp. 319–415.
4. Carcione, J. M., Kosloff, D., Behle, A. and Serian, G., 1992, A spectral scheme for wave propagation simulation in 3-D elastic-anisotropic media: *Geophysics*, 57, pp. 1593–1607.
5. Fornberg, B., 1988, The pseudospectral method: Accurate representation of interfaces in elastic wave calculations: *Geophysics*, 53, pp. 625–637.
6. Fornberg, B., 1987, The pseudospectral method: Comparisons with finite difference for the elastic wave equation: *Geophysics*, 52, pp. 483–501.
7. Fornberg, B. and Sloan, D. M., 1994, A review of pseudospectral methods for solving partial differential equations: *Acta Numerica*, pp. 203–267.
8. Gottlieb, D., Gunzburger, M. and Turkel, E., 1982, On numerical boundary treatment of hyperbolic systems for finite difference and finite element methods: *SIAM Journal of Numerical Analysis*, 19, pp. 671–682.
9. R.-D. Jih, 1994, Numerical Modeling of Crustal Phase Propagation in Irregular Waveguides, 16th PL/AFOSR Seismic Symposium, pp. 173-81. PL-TR-94-2217, ADA284667

10. Nielsen, P., Flemming, I., Berg, P. and Skovgaard O., 1994, Using the pseudospectral technique on curved grids for 2D acoustic forward modeling: *Geophysical Prospecting*, **42**, pp. 321–341.
11. Kosloff, D., Kessler, D., Filho, A. Q., Tessmer, E., Behle, A. and Strahilevitz, R., 1990, Solution of the equations of dynamic elasticity by a Chebychev spectral method: *Geophysics*, **55**, pp.734–748.
12. Kindelan, M., Kamel, A. and Sguazzero, P., 1990, On the construction and efficiency of staggered numerical differentiators for the wave equation: *Geophysics*, **55**, pp. 107–110.
13. Sheriff, R. E., and Geldart, L. P., 1982, *Exploration Seismology*, Vol. 1: *History, Theory and Data Acquisition*, Cambridge, Cambridge University Press.
14. Sheriff, R. E. and Geldart, L. P., 1983, *Exploration Seismology*, Vol. 2: *Data-processing and Interpretation*, Cambridge, Cambridge University Press.
15. Tessmer, E. and Kosloff, D., 1994, 3-D elastic modeling with surface topography by a Chebyshev spectral method: *Geophysics*, **59**, pp. 464–473.
16. Tessmer, E., Kosloff, D. and Behle, A., 1992, Elastic wave propagation simulation in the presence of surface topography: *Geophysical Journal International*, **108**, pp. 620–632.
17. Meng, Z., Feng, Y. and Fan, Z., 1992, Radiation boundary conditions for complicated wave propagations: *Chinese Journal of Geophysics*, **34**, pp.509–516.
18. Fan, Z. and Teng, Y., 1988, Numerical simulations of viscoelastic waves: *Acta Geophysica Sinica*, **31**, pp. 198–209.

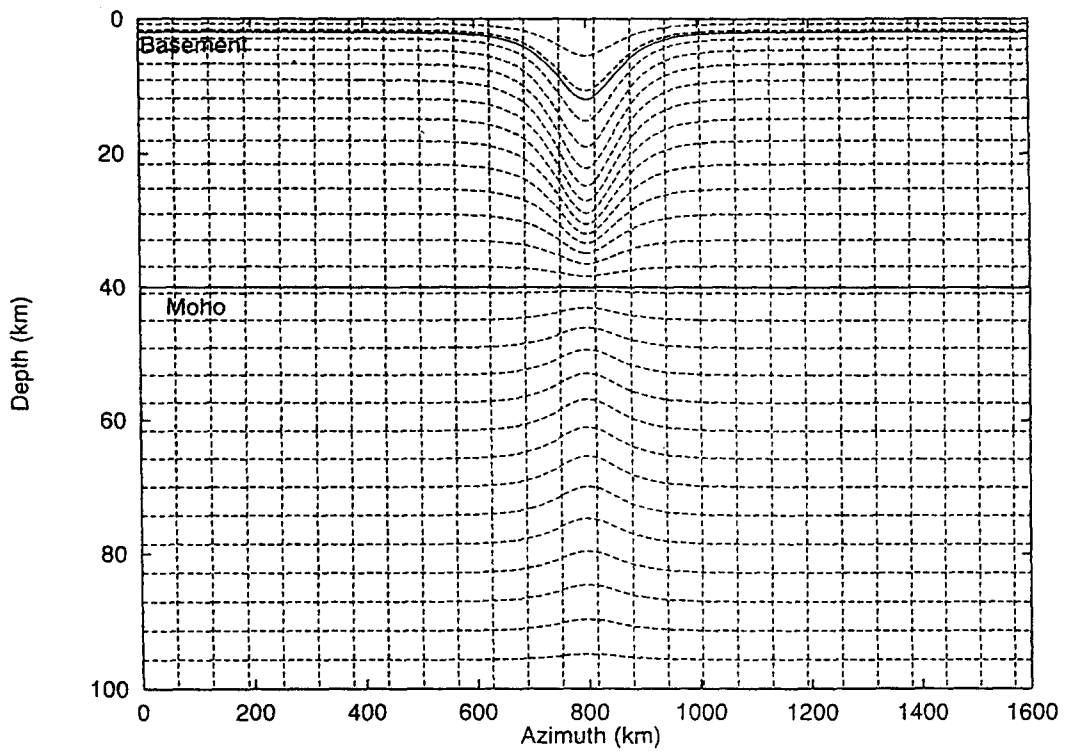


Fig. 1. Deep sedimentary basin model, showing eta grid lines conforming to the major contours, and eta spacing proportional to travel time.

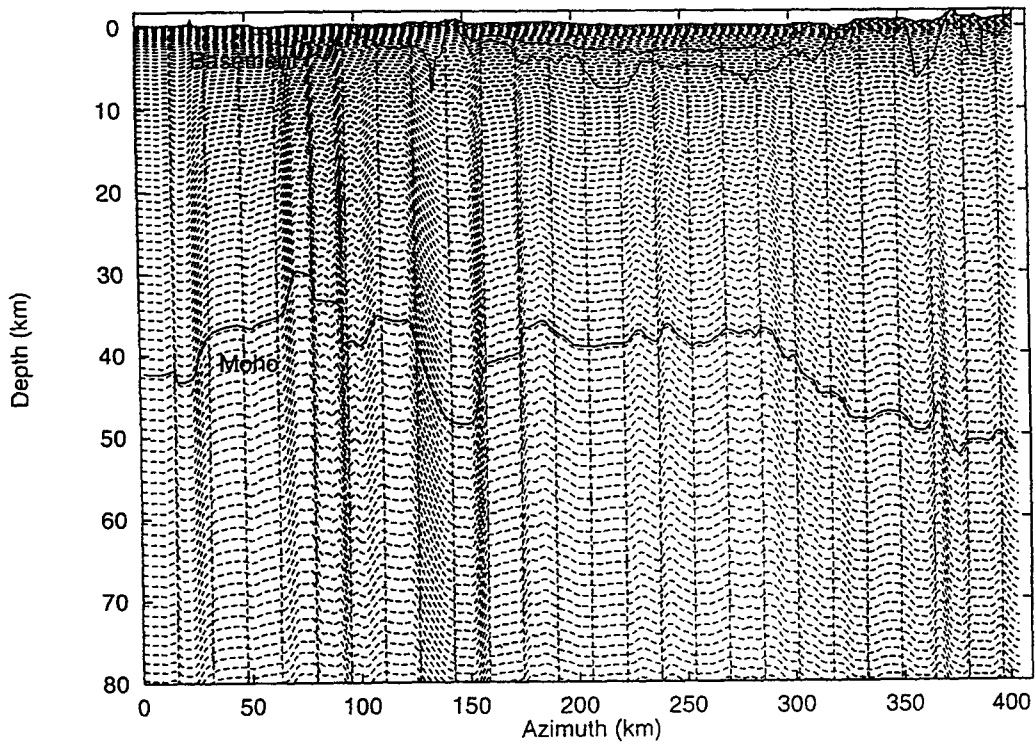
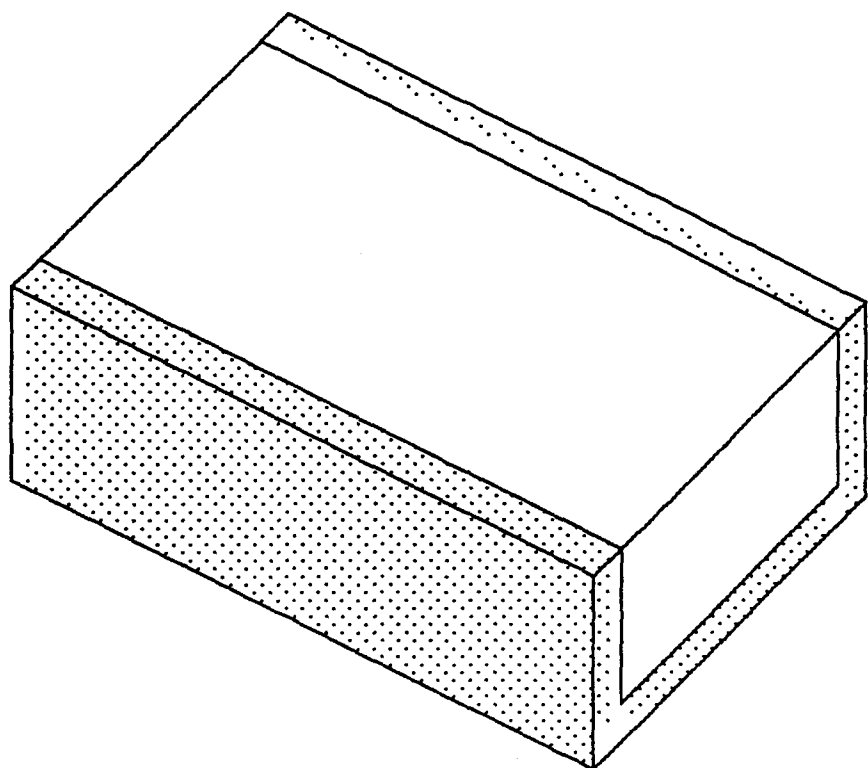
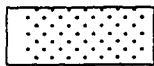


Fig. 2. Trans-Urals Soviet DSS model.



Active Computational Region



Attenuating Layer

Figure 3. Sketch of three-dimensional computational domain showing attenuating layers at bottom and sides.